Mean-field solution of the neural dynamics in a Greenberg-Hastings model with excitatory and inhibitory units

Joaquin Almeira,[1,2,3] Tomas S. Grigera,[2,4,5,6] Daniel A. Martin,[2,7] Dante R. Chialvo,[2,7] and Sergio A. Cannas[1,2,3]

[1]*Instituto de Física Enrique Gaviola (IFEG-CONICET), Facultad de Matemática Astronomía Física y Computación, Universidad Nacional de Córdoba, 5000 Córdoba, Argentina*

[2]*Consejo Nacional de Investigaciones Científcas y Tecnológicas (CONICET), 1425 Buenos Aires, Argentina*

[3]*Facultad de Matemática Astronomía Física y Computación, Universidad Nacional de Córdoba, 5000 Córdoba, Argentina*

[4]*Instituto de Física de Líquidos y Sistemas Biológicos (IFLYSIB), CONICET and Universidad Nacional de La Plata, 1900 La Plata, Argentina*

[5]*Departamento de Física, Facultad de Ciencias Exactas, Universidad Nacional de La Plata, 1900 La Plata, Argentina*

[6]*Istituto dei Sistemi Complessi, Consiglio Nazionale delle Ricerche, 00185 Rome, Italy*

[7]*Instituto de Ciencias Físicas (ICIFI-CONICET), Center for Complex Systems and Brain Sciences (CEMSC3), Escuela de Ciencia y Tecnología, Universidad Nacional de Gral. San Martín, Campus Miguelete, San Martín, 1650 Buenos Aires, Argentina*

(Received 19 February 2024; accepted 26 June 2024; published 19 July 2024)

We present a mean-field solution of the dynamics of a Greenberg-Hastings neural network with both excitatory and inhibitory units. We analyze the dynamical phase transitions that appear in the stationary state as the model parameters are varied. Analytical solutions are compared with numerical simulations of the microscopic model defined on a fully connected network. We found that the stationary state of this system exhibits a first-order dynamical phase transition (with the associated hysteresis) when the fraction of inhibitory units f is smaller than some critical value $f_t \lesssim 1/2$, even for a finite system. Moreover, any solution for $f < 1/2$ can be mapped to a solution for purely excitatory systems ($f = 0$). In finite systems, when the system is dominated by inhibition ($f > f_t$), the first-order transition is replaced by a pseudocritical one, namely a continuous crossover between regions of low and high activity that resembles the finite size behavior of a continuous phase transition order parameter. However, in the thermodynamic limit (i.e., infinite-system-size limit), we found that $f_t \to 1/2$ and the activity for the inhibition dominated case ($f \geqslant f_t$) becomes negligible for any value of the parameters, while the first-order transition between low- and high-activity phases for $f < f_t$ remains.

DOI: 10.1103/PhysRevE.110.014130

I. INTRODUCTION

The theory of phase transitions in systems under thermodynamical equilibrium is a well-established statistical mechanic's formalism. Conversely, the analogous phenomena in nonequilibrium systems present a much richer scenario that appears to be more complex to formalize, so a general theory is still lacking [1,2]. In particular, critical phenomena and phase transitions in nonequilibrium systems seem to be more sensitive to the microscopic details (i.e., the dynamic rules) than the equilibrium counterpart. In other words, universality seems to be more restricted in nonequilibrium systems than in thermodynamical ones, one of the reasons behind the larger variety of observed behaviors [1–3]. Hence, the path towards the development of a general theory of the topic at the present strongly relies on comparing the behavior of as many different models as possible, with the as deep as possible understanding of them.

In this work, we considered a basic model of neural dynamics with excitatory and inhibitory units introduced in Ref. [4], which is indeed a generalization of a previous model [5–7] based on Greenberg-Hastings (GH) cellular automaton of excitable media [8]. This model has shown recently a very rich phase transitions scenario [4–7] and provided support to the "brain criticality hypothesis" [9–11] (for recent reviews on the topic, see, e.g., Refs. [12–14]). But besides its interest in neuroscience, the complexity exhibited by the model highlights its importance *per se* to the field of nonequilibrium phase transitions theory. Up to now, all the studies of this model were based on numerical simulations. Here we present the mean-field solution of the previously considered model in Ref. [4], in the sense of running the same local dynamical rules in a fully connected network, which allows us to obtain a set of differential equations for the average population densities of active neurons. Mean-field solutions are always of theoretical interest, not only because analytical expressions are a powerful tool that allow a deeper understanding of the problem but also because they provide us with some limit cases to check the results of models defined on more realistic networks.

We obtained a set of differential equations for the average population densities of excited sites and focused our analysis on the stationary solutions of those equations, both for finite-size systems and in the infinite-size limit. For excitatory units only, we found a discontinuous transition with hysteresis. For networks with a moderate fraction of inhibitory units, we found that the solutions can be mapped to solutions for networks of purely excitatory units, after rescaling the relevant variables, while a negligible activity was found if there are more inhibitory than excitatory units.

The paper is organized as follows. In Sec. II we present the model and describe the stochastic technique used to estimate

the mean-field dynamical equations. In Sec. III we analyze the stationary solutions of the mean-field equations in the parameter space and compare them with some numerical simulations of the fully connected model. A general discussion of the results is presented in Sec. IV.

II. MODEL AND METHODS

In the model considered here, a three-state dynamical variable $x_i = 0,\ 1,\ 2$ is associated to each node i of some complex network, representing the following dynamical states: quiescent ($x_i = 0$), excited ($x_i = 1$), and refractory ($x_i = 2$). Also to each node i there is associated a quenched random variable $\epsilon_i = \pm 1$, representing an excitatory or inhibitory unit, respectively. There is a fraction f of inhibitory units in the network, namely each node has a probability f to be inhibitory ($\epsilon = -1$) and $1 - f$ to be excitatory ($\epsilon = +1$). The model follows a parallel dynamics in a discrete time t, already described in previous articles [4–7], namely (a) each quiescent neuron can become excited with a small spontaneous activation probability r_1, or if the sum of their active neighbors, weighted through the connectivity matrix, surpasses an activation threshold T (the control parameter of this model), which is the same for all neurons; (b) active neurons become refractory after one step; and (c) refractory neurons become quiescent with probability r_2 per unit time (so, the average refractory period has a duration of $1/r_2$). The transition probabilities for the i th site are given by

$$\begin{aligned} P_i(0 \to 1) &= 1 - (1 - r_1)\left\{1 - \Theta\left[\sum_j W_{ij}\epsilon_j \delta(x_j, 1) - T\right]\right\} \\ P_i(1 \to 2) &= 1 \\ P_i(2 \to 0) &= r_2, \end{aligned} \tag{1}$$

where Θ is the Heaviside function and $\delta(x, y)$ is the Kroenecker delta function. W_{ij} is a symmetric synaptic matrix, and the sum is performed over the nearest neighbors of the node i. To simplify reading, Tables I and II, containing a list of variables, are included in Appendix A.

A first version of this model with purely excitatory neurons $f = 0$ was introduced by Haimovici *et al.* [5]. The synaptic matrix W_{ij} in this case was constructed based on an empirical structure of neuroanatomical connections of about $N \sim 1000$ nodes [15]. The consequent analysis of cluster statistics provided the first evidence of critical behavior in this model [5]. Further evidence about criticality was obtained through the implementation of the model on small world networks (Watts-Strogatz model) with arbitrary size N (still with $f = 0$). Such implementation allowed to perform a finite-size scaling analysis [6]. Moreover, a very rich dynamical phase diagram emerged as the topological properties of the network (namely the average degree $\langle k \rangle$ and the rewiring probability) were varied [6,7]. Subsequent analyses over synthetic, finite-degree networks considered a weight distribution that mimicked the neuroanatomical one, specifically, the non-null synaptic weights were quenched random variables with an exponential distribution

$$p(W_{ij} = w) = \beta e^{-\beta w}. \tag{2}$$

Furthermore, the inclusion of inhibitory units $f \neq 0$ to the previous model revealed the possibility of tricritical behavior in the (f, T) space, depending on the topology of the network [4].

In this work, we consider the implementation of the model on a fully connected network of N units (consequently, its degree is $N - 1$). As usual in this kind of system, interactions have to be rescaled by N to prevent neurons from receiving a diverging input in the $N \to \infty$ limit. Therefore, instead of W, we consider a synaptic matrix $W \to w$, with

$$w_{ij} = w_{ji} = \frac{1}{N} W_{ij}, \tag{3}$$

for all pairs of nodes (i, j) with $w_{ii} = 0$ (no self-connections) and $p(W_{ij})$ given by Eq. (2). The values of W (or w) are randomly chosen at the beginning of the simulation and remain fixed (i.e., quenched disorder). In order to be consistent with previous results (Refs. [4,6,7]) we also use the values $r_1 = 10^{-3}$ and $r_2 = 0.3$ and $\beta = 12.5$.

For long-enough timescales it is expected the evolution of this model to be well described as a continuous time Markov stochastic process in the variables $\vec{x}(t) = (x_1(t), \ldots, x_N(t))$, with appropriated chosen transition rates between states. Following usual procedures [16], a Focker-Planck equation can be derived through a Kramers-Moyal expansion, which in turn allows us to obtain stochastic Langevin equations for the population densities $\rho_{e/r}$ and $\psi_{e/r}$, where

$$\rho_e = \frac{1}{N}\left\langle \sum_{i \in \text{exc.}} \delta(x_i, 1) \right\rangle, \quad \rho_r = \frac{1}{N}\left\langle \sum_{i \in \text{exc.}} \delta(x_i, 2) \right\rangle,$$
$$\psi_e = \frac{1}{N}\left\langle \sum_{i \in \text{inh.}} \delta(x_i, 1) \right\rangle, \quad \psi_r = \frac{1}{N}\left\langle \sum_{i \in \text{inh.}} \delta(x_i, 2) \right\rangle.$$

$\rho_{e/r}$ is the density of neurons that are simultaneously excitatory and active (e) or refractory (r), respectively, $\psi_{e/r}$ is the density of simultaneously inhibitory and active or refractory neurons, and $\langle ... \rangle$ is the average over disorder. The necessary steps are described in detail in Appendix B. The derivation followed closely similar calculations in a related in Refs. [17,18]. After some simplifications, we obtained the following dynamical equations:

$$\dot{\rho}_e = (1 - f - \rho_e - \rho_r) \times \left\{\mu_1 + \eta\left[\frac{\omega(\rho_e - \psi_e) - T}{\sigma}\right]\right\} - \mu_3 \rho_e, \tag{4a}$$

$$\dot{\rho}_r = \mu_3 \rho_e - \mu_2 \rho_r, \tag{4b}$$

$$\dot{\psi}_e = (f - \psi_e - \psi_r) \times \left\{\mu_1 + \eta\left[\frac{\omega(\rho_e - \psi_e) - T}{\sigma}\right]\right\} - \mu_3 \psi_e, \tag{4c}$$

$$\dot{\psi}_r = \mu_3 \psi_e - \mu_2 \psi_r, \tag{4d}$$

where

$$\mu_1 = \frac{r_1}{1 - r_1}, \quad \mu_2 = \frac{r_2}{1 - r_1}, \quad \mu_3 = \frac{1}{1 - r_1} \tag{5}$$

(see Appendix C). $\omega \equiv \langle W_{ij} \rangle$ [from Eq. (1), we get $\omega = 1/\beta$], and σ is the standard deviation of the argument of the Heaviside function in Eq. (1) and it measures the neuron's input variability. We verified that $\sigma^2 \sim 1/N$ (and consequently

$\sigma \to 0$ in the thermodynamic limit) on numerical simulations of the microscopic model for different values of f and T (see Appendix D). $\eta(x)$ is some sigmoid function monotonically going from 0 (for $x \to -\infty$) to 1 (for $x \to \infty$). We have chosen

$$\eta(x) = \frac{e^{2x}}{1+e^{2x}}. \tag{6}$$

We focused on the stationary solutions of Eqs. (4a)–(4d) (with their corresponding stability) and the dynamical phase transition between them in the (f, T) space. The solutions were obtained analytically, when possible, and numerically using fourth-order Runge-Kutta method when needed.

We also made some comparisons between stationary values of ρ_e and ψ_e obtained by solving numerically the model with $\sigma \neq 0$ and numerical simulations of the microscopic model on a fully connected network.

III. RESULTS

We studied the stationary solutions of Eqs. (4a) and (4b) for small but different from zero values of σ and then we analyzed the thermodynamic limit $\sigma \to 0$.

A. Purely excitatory neurons ($f = 0$)

We first analyzed the particular case $f = 0$, i.e., a system with no inhibitory units. When $f = 0$ we have $\psi_e = \psi_r = 0$ and Eqs. (4a) and (4b) reduce to

$$\begin{aligned} \dot{\rho}_e &= (1-\rho_e-\rho_r)\left[\mu_1 + \eta\left(\frac{\omega\rho_e - T}{\sigma}\right)\right] - \rho_e\mu_3 \\ \dot{\rho}_r &= \rho_e\mu_3 - \rho_r\mu_2. \end{aligned} \tag{7}$$

A combination of Eqs. (7) and (5) reproduces previous results by Barzon and coauthors [18]. Notice that the stationary solutions of Eqs. (7) are constrained to an interval $(\rho_e^{\min}, \rho_e^{\max})$, where the limiting values are those for which $\eta(..) = 0$ and 1 respectively and are given by

$$\rho_e^{\min} = \frac{\mu_1\mu_2}{S}, \tag{8}$$

and

$$\rho_e^{\max} = \frac{\mu_2(1+\mu_1)}{S+\mu_2+\mu_3}, \tag{9}$$

where $S = \mu_1\mu_2 + \mu_2\mu_3 + \mu_3\mu_1$. Notice that these values are independent of σ. Assuming $r_1 \ll 1$, we get $\rho_e^{\min} = \frac{r_1 r_2}{r_1+r_2+r_1 r_2} \simeq r_1$: The minimum activity corresponds to the spontaneous activation solely. Similarly, we get $\rho_e^{\max} = \frac{r_2}{2r_2+1} = (2+1/r_2)^{-1}$, as expected.[1] These results are in complete agreement with previous ones [18,19].

To study the stationary states of Eqs. (7) and their stability, we analyzed the associated nullclines, i.e., the curves defined by the conditions $\dot{\rho}_r = 0$ and $\dot{\rho}_e = 0$, whose intersections give the corresponding fixed points. The typical behavior of the nullclines is shown in Fig. 1 for different values of σ. The curve corresponding to $\dot{\rho}_r = 0$ is a straight line

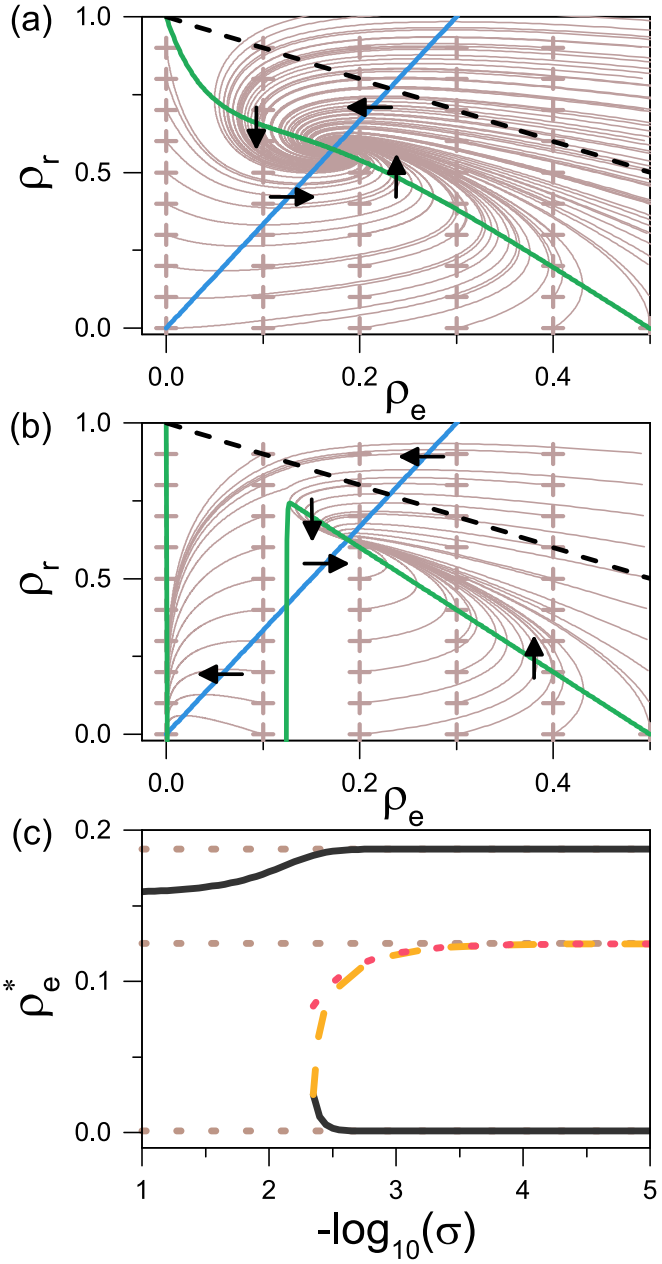

FIG. 1. Stationary solutions of the dynamical equations considering only excitatory units ($f = 0$). (a) Phase portrait for threshold $T = 0.01$ and neuron input variability $\sigma = 10^{-2}$ showing the evolution of the density of active (ρ_e) and refractory (ρ_r) neurons. Thick blue line corresponds to the nullcline $\dot{\rho}_r = 0$, while the green line corresponds to $\dot{\rho}_e = 0$. Black arrows show the flow directions at the nullclines. Several trajectories starting at the + signs are shown in brown. The black dashed line delimits the area of physically relevant solutions ($\rho_e + \rho_r < 1$). (b) Same as (a) for $\sigma = 10^{-4}$. (c) Stationary solutions as a function of σ. Black lines correspond to stable solutions while orange dashed lines correspond to unstable solutions. The red dashed line corresponds to the polynomial approximation of ρ^{mid} discussed in the Appendix E. From top to bottom, dotted lines correspond to $\rho_e^{\max}$, $\frac{T}{\omega}$, and $\rho_e^{\min}$.

[1]This last result can be easily understood if each single neuron fires at its maximum rate: It will spend 1 step in the excited state, on average, $1/r_2$ steps in the refractory state, and after that, just one step in the quiescent state before starting the cycle again. So the cycle lasts on average $2 + 1/r_2$ steps, and the neuron spends one step per cycle (i.e., $\frac{1}{2+1/r_2}$ of the time) in the excited state.

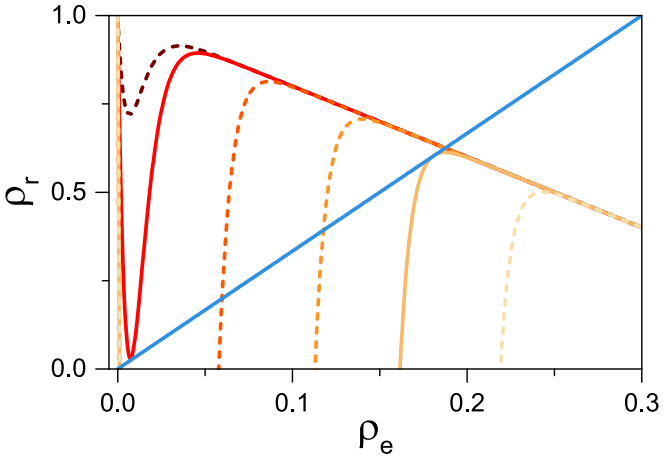

FIG. 2. Stationary solutions for different values of the threshold T considering only excitatory units ($f = 0$). The lines show nullclines of the dynamical equations for input variability $\sigma = 10^{-3}$. The blue line corresponds to the nullcline of refractory neuron density, $\dot{\rho}_r = 0$, while the other lines correspond to active neuron density, $\dot{\rho}_e = 0$, for different values of T, increasing from left to right: 0.0024, 0.003093, 0.006, 0.01, 0.01365, and 0.018. The full line nullclines correspond to the limiting values ($T_{\min}$, $T_{\max}$), respectively, such that the system presents three fixed points only when $T_{\min} < T < T_{\max}$.

$\rho_r^* = \rho_e^* \mu_3/\mu_2$, where the asterisk holds for stationary solutions (or long time averages in the numerical model). The curve corresponding to $\dot{\rho}_e = 0$ exhibits a nonmonotonous behavior for several values of σ and T.

For relatively large values of σ, and for any value of T, we have only one fixed point, which is stable [see Fig. 1(a)]. As σ is decreased, we find several values of T for which there are three fixed points, two stable and one unstable in between [see Fig. 1(b)]. The new solutions are generated through a perturbed pitchfork bifurcation.

Finally, in the limit $\sigma \to 0$, the stable solutions converge to $\rho_e^{\min}$ and $\rho_e^{\max}$, given by Eqs. (8) and (9). The unstable solution ρ^{mid} is close to $\frac{T}{\omega}$. Indeed, an estimate of its value can be obtained expanding Eqs. (7) about $\rho_e = \frac{T}{\omega}$, see the Appendix E.

Multiple solutions can be found also as a function of T. The nullclines for fixed σ and several values of T are shown in Fig. 2. We observe a range of values $T_{\min} \leqslant T \leqslant T_{\max}$ for which there are three fixed points. Outside such a range of values of T, there is only one stable fixed point. Such behavior is characteristic of a discontinuous transition with bistability, and the presence of hysteresis is expected.

We verified the presence of hysteresis and consequently bistability, by performing a loop of increasing-decreasing T and solving Eqs. (7) using the Runge-Kutta (RK) method. For each value of T, we run the RK algorithm until the system reaches a stationary state and record the stationary value of ρ_e before changing $T \to T \pm \Delta T$ ($\Delta T \sim 1.5 \times 10^{-5}$) and restart the RK algorithm with the previous state as the new initial condition. We also performed a similar calculation using the cellular automaton defined by Eqs. (1) in a fully connected network. In this case, for every value of T, we discard the first $t = 500$ steps and average the fraction of active sites over 10^3–10^4 steps before changing T. In both cases, we observed a clear hysteresis loop. The whole phenomenology can be observed for a wide range of variations of the parameters ($\mu_1, \mu_2, \mu_3, \sigma$) and has also been reported for the same cellular automaton on a Watts-Strogatz network with average degree $20 < \langle k \rangle < 40$ and large-enough values of the network rewiring probability [6,7].

B. Excitatory and inhibitory neurons

We next considered the general case $f \neq 0$. In this case, we deal with four equations; nevertheless, we can define the following change of variables:

$$\Delta_{e/r} = f\,\rho_{e/r} - (1-f)\psi_{e/r}$$
$$\Sigma_{e/r} = \rho_{e/r} + \psi_{e/r}. \tag{10}$$

Σ_e represents the activity, that is the total fraction of active units, independently of whether they are excitatory or inhibitory, and Σ_r is the same for refractory units. $\Delta_{e/r}$ are auxilliary variables. The evolution equations for $\Delta_{e/r}$ can be written as:

$$\dot{\Delta}_e = (-\mu_3 - \mathcal{N})\Delta_e - \mathcal{N}\Delta_r, \tag{11a}$$
$$\dot{\Delta}_r = \mu_3\Delta_e - \mu_2\Delta_r, \tag{11b}$$

where the auxiliary variable $\mathcal{N}$ containing the nonlinear terms is $\mathcal{N} \doteq \mu_1 + \eta(\frac{\omega(\rho_e - \psi_e) - T}{\sigma}) > 0$, and $\rho_e - \psi_e$ can be written as $(1-2f)\Sigma_e + 2\Delta_e$. It is straightforward to notice that $\Delta_e = \Delta_r = 0$ is a solution of Eqs. (11) in the stationary state. Moreover, it can be shown that it is the only solution and that it is locally stable (see Appendix F). This means that $\Delta_{e/r}$ monotonically decay to zero. Consequently, after a transient, we have $\Delta_{e/r} = 0$ and $\psi_{e/r} = \rho_{e/r}\frac{f}{1-f}$, which is reasonable since each inhibitory neuron receives, on average, the same stimulus as each excitatory neuron. We have verified that this decay holds both in the model equations and in the numerical simulations. The equations for $\Sigma_{e/r}$, after setting $\Delta_{e/r} = 0$, read:

$$\dot{\Sigma}_e = (1 - \Sigma_e - \Sigma_r) \times \left\{\mu_1 + \eta\left[\frac{\omega(1-2f)\Sigma_e - T}{\sigma}\right]\right\} - \Sigma_e\mu_3, \tag{12a}$$
$$\dot{\Sigma}_r = \Sigma_e\mu_3 - \Sigma_r\mu_2. \tag{12b}$$

Notice that Eqs. (12) for $\Sigma_{e/r}$ are the same as Eqs. (7) for $\rho_{e/r}$ in the purely excitatory case, after rescaling $T \to T/(1-2f)$ and $\sigma \to \sigma/(1-2f)$. We can also rewrite Eqs. (12) in terms of the excitatory units activity, since $\rho_{e/r} = \Sigma_{e/r}(1-f)$. In particular, Eqs. (8) and (9) now read:

$$\Sigma_e^{\min} = \frac{\mu_1\mu_2}{S}, \tag{13}$$

and

$$\Sigma_e^{\max} = \frac{\mu_2(1+\mu_1)}{S+\mu_2+\mu_3}, \tag{14}$$

or, equivalently,

$$\rho_e^{\min} = (1-f)\frac{\mu_1\mu_2}{S} \tag{15}$$
$$\rho_e^{\max} = (1-f)\frac{\mu_2(1+\mu_1)}{S+\mu_2+\mu_3}. \tag{16}$$

We verified that these rescaling results also hold for the stationary solutions (Σ_e^*, Σ_r^*) of Eqs. (12a) and (12b) obtained

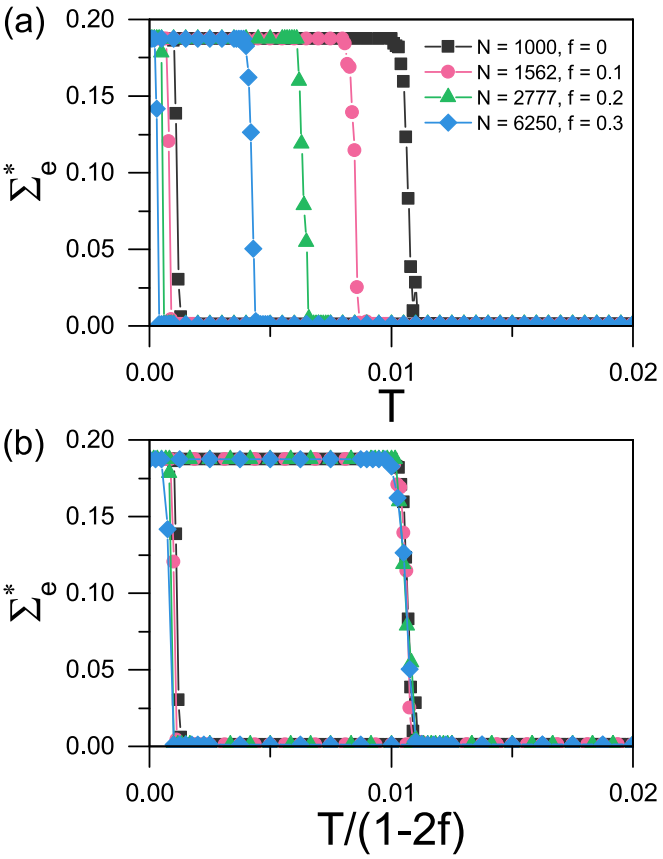

FIG. 3. Stationary activity Σ_e^* in numerical simulations of the microscopic model, for different values of the fraction of inhibitory units $f < 1/2$. (a) Σ_e^* as a function of the threshold T for several values of f, in systems of size $N = \frac{N_0}{(1-2f)^2}$ with $N_0 = 1000$. (b) Same data as in (a) as a function of $T/(1-2f)$.

from numerical simulations for finite N (see Fig. 3). Since $\sigma^2 \sim \frac{1}{N}$ (see Appendix D), we considered systems of size $\frac{N_0}{(1-2f)^2}$ with $N_0 = 1000$.

For $f \geqslant 1/2$, Eq. (12a) predicts that the fraction of active neurons Σ_e will decrease as σ decreases, converging to the minimum possible value Eq. (13) in the limit $\sigma \to 0$, for any value of T.

The stationary solutions of Eqs. (12a) and (12b) satisfy $\Sigma_r^* = \Sigma_e^* \mu_3/\mu_2$ and

$$T = R(\Sigma_e^*, f) \tag{17}$$

where

$$R(\Sigma_e, f) = \frac{\sigma}{2} \ln\left[\frac{\mu_2 - (\mu_2+\mu_3)\Sigma_e}{S\Sigma_e - \mu_1\mu_2} - 1\right] + \omega(1-2f)\Sigma_e. \tag{18}$$

From Eq. (18), we find that the bistability limits in the thermodynamic limit ($\sigma \to 0$ in the model, or $N \to \infty$ in the numerical simulations) are as follows:

$$T_{\min/\max} = \omega(1-2f)\Sigma_e^{\min/\max}, \tag{19}$$

having then a finite range of T values where there is bistability. For finite N, we find that $T_{\min/\max}$ converge rather slowly (as a power law) to the values given by Eq. (19) (see Appendix E).

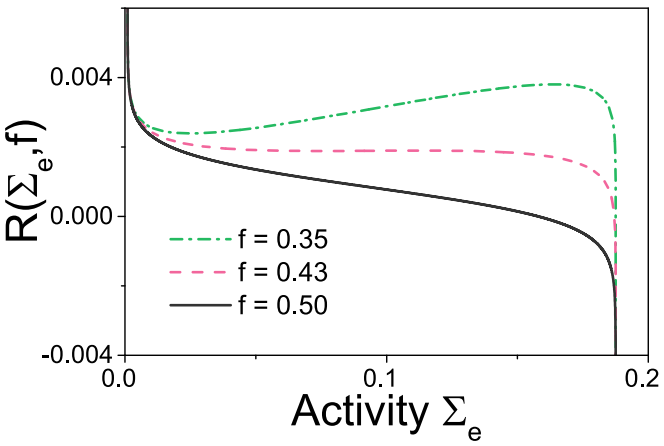

FIG. 4. Typical behavior of $R(\Sigma_e, f)$ as a function of the activity Σ_e for input variability $\sigma = 10^{-3}$ and different values of the fraction of inhibitory units f.

The typical behavior of $R(\Sigma_e, f)$ as a function of Σ_e is shown in Fig. 4. When $\sigma \ll 1$, the behavior of R as a function of Σ_e is dominated by the linear term proportional to ω, except for values of ρ_e very close to $\Sigma_e^{\min}$ or $\Sigma_e^{\max}$. Since $\omega(1-2f)$ changes of sign at $f = 1/2$, we see that there exists a value $f_t \approx 1/2$, such that when $f < f_t$, $R(\Sigma_e, f)$ has a positive slope and Eq. (17) has three solutions that converge to the previous analyzed ones (i.e., when $f \to 0$). Hence, one could expect a discontinuous transition between low- and high-activity phases and hysteresis in the whole range $f < f_t$. Conversely, when $f \geqslant f_t$, there is only one solution that changes continuously from high values of the activity for small values of T to small activities for high values of it.

Numerical solutions of Eqs. (4a)–(4d) analog to those performed for $f = 0$ (i.e., cycling T) support the above conclusions. The corresponding results for the stationary values of the total activity $\Sigma_e^* = \rho_e^* + \psi_e^*$ as a function of T for different values of f and a finite but small value of σ are shown in Fig. 5. The behavior of the activity when $f > f_t$ is consistent with the expected finite-size behavior of a second-order phase transition order parameter, at least for values of f close to f_t. In that sense, the end point of the discontinuous transition line $(f, T) = (f_t, T_t)$ could be regarded as a tricritical one. However, we will show that such pseudocritical behavior for $f > f_t$ completely disappears in the thermodynamic limit $\sigma \to 0$.

The pseudotricritical values f_t and Σ_e^t correspond to an inflexion point of $R(\Sigma_e, f)$. So equating the first and second derivatives of Eq. (18) to zero and solving together with Eq. (18) we obtain after some algebra

$$\Sigma_e^t = \frac{\mu_1\mu_2(S+\mu_2+\mu_3) + S(\mu_2+\mu_1\mu_2)}{2S(S+\mu_2+\mu_3)}, \tag{20}$$

$$f_t = \frac{1}{2} - \frac{\sigma}{4\omega}B, \tag{21}$$

$$T_t = \frac{\sigma}{2}\left\{\Sigma_e^t B + \ln\left[\frac{\mu_2 - (\mu_2+\mu_3)\Sigma_e^t}{S\Sigma_e^t - \mu_1\mu_2} - 1\right]\right\}, \tag{22}$$

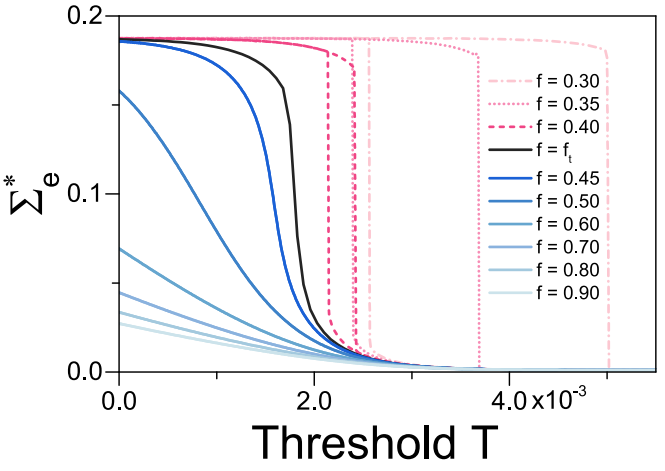

FIG. 5. Stationary activity (excitatory and inhibitory neurons) during a cycling process of the threshold T, obtained from numerical solutions of Eqs. (4) for $\sigma = 10^{-3}$ and different values of the fraction of inhibitory units f. A clear hysteresis (red curves) is observed for $f < f_t$. For $f > f_t$ there is no hysteresis and the system exhibits a continuous crossover (solid blue lines) between a low-activity regime (for high T) to a high-activity one (low values of T).

where

$$B = \frac{4S(S + \mu_2 + \mu_3)}{\mu_2^2 \mu_3}$$

and T_t is the corresponding pseudotricritical threshold value. In the thermodynamic limit $\sigma \to 0$ we see that $f_t \to 1/2$ and $T_t \to 0$. To understand the last result we calculated again the numerical solutions of the dynamical equations in cycling process of T, for a sequence of decreasing values of σ and values of f around $1/2$. The main results of these calculations are shown in Fig. 6. We see that in the limit $\sigma \to 0$ the global activity becomes negligible ($\sim \rho_e^{\min} \sim 0.5 \times 10^{-3}$ in the present case) for any value of $T > 0$ when $f \geqslant 1/2$, while a well defined hysteresis loop is established when $f < 1/2$. Consistently, we obtained the same results when simulating the microscopic model in a fully connected network, following the same cycling protocol for increasing values of the system size N (every curve was averaged in this case over the quenched disorder in both the synaptic weights and the distribution of inhibitory units), as shown in Fig. 7. Extrapolation of these curves to $N \to \infty$ (not shown) when $f \geqslant 1/2$ confirms that the activity becomes negligible for any value of $T > 0$.

This result can be understood in the following way. Since for $f > 1/2$ there are more inhibitory than excitatory neurons, in a fully connected network, any number of excitatory active neurons at time t will activate (on average) more inhibitory than excitatory units at time $t + 1$, which will make the total activity decrease at time $t + 2$. Hence, global activity is expected to decrease monotonically in the long term and the only possible activity for $f > 1/2$ in the stationary state is due to the finite-size fluctuations in the number of active excitatory and inhibitory units, which is only relevant for small N. A phase diagram in the thermodynamic limit is shown in Fig. 8.

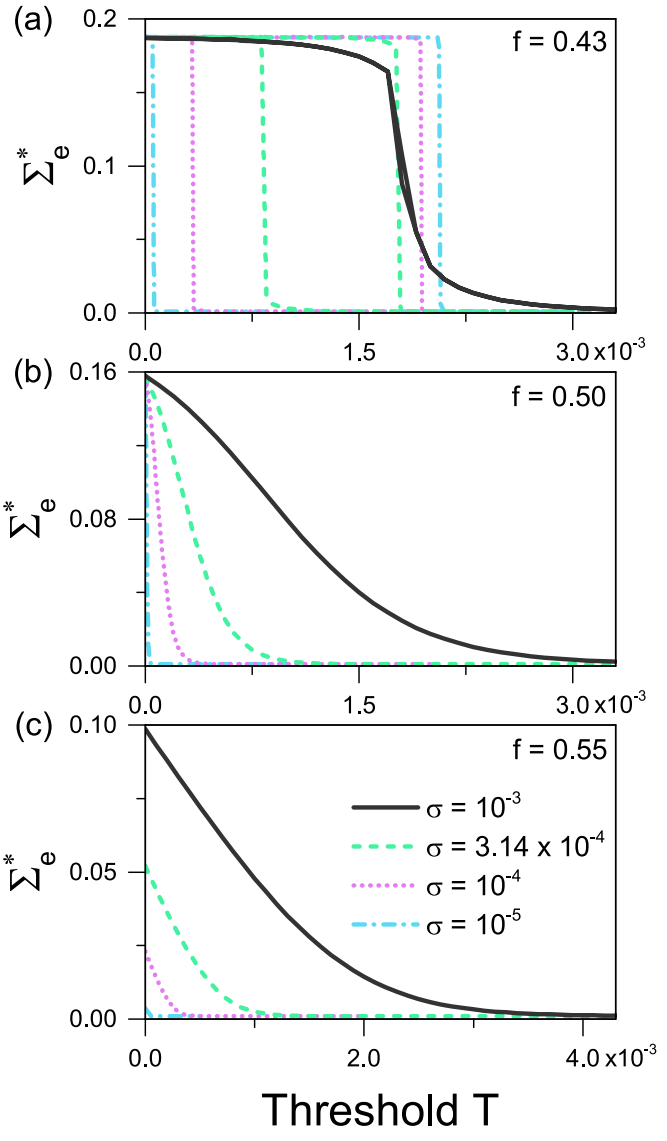

FIG. 6. Stationary activity during a cycling process of the threshold T, obtained from numerical solutions of Eqs. (4) when the input variability $\sigma \to 0$ for values of the fraction of inhibitory units f around $1/2$.

IV. DISCUSSION

A. Summary of the results

We obtained the mean-field dynamical equations of a Greenberg-Hastings neural model with excitatory and inhibitory units. The dynamical equations results and the numerical simulation of model show a very good agreement. The analysis of the stationary solutions revealed the existence of a first-order (i.e., discontinuous) dynamical phase transition between an active phase (high values of the total activity Σ_e^*) and an inactive one (low values of the total activity Σ_e^*), where the threshold T plays the role of the control parameter of the transition. Such transition happens for values of the inhibitory neurons fraction f smaller than certain value $f_t \leqslant 1/2$, even for finite systems, and remains in the thermodynamic limit $\sigma \to 0$, where $f_t \to 1/2$.

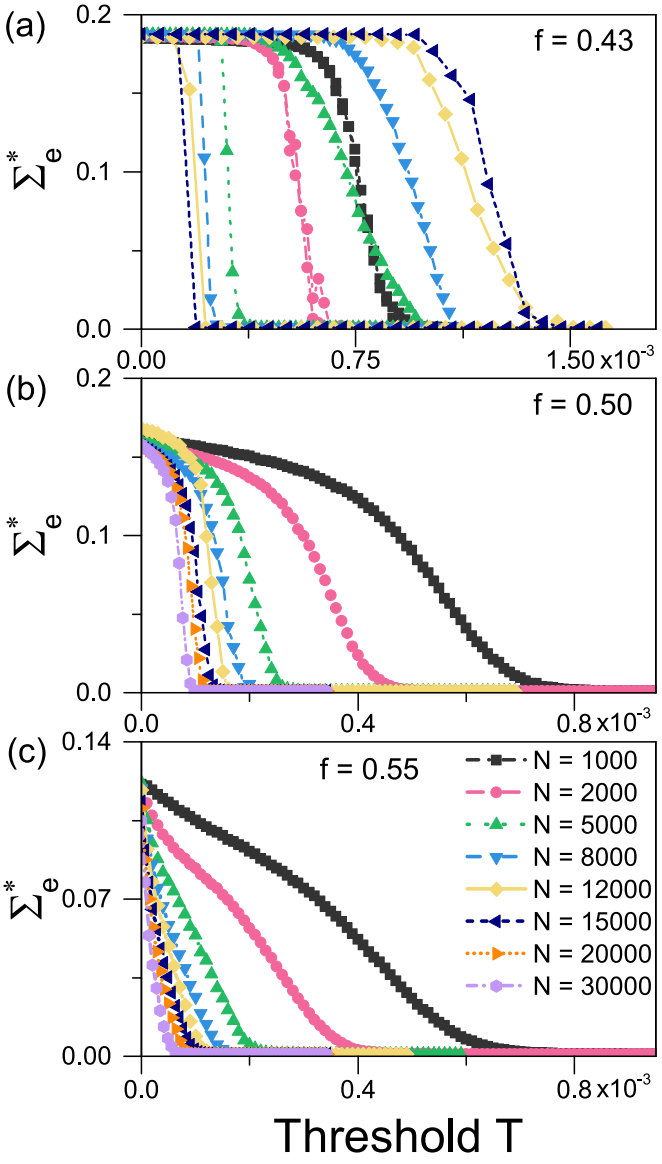

FIG. 7. Average stationary activity during a cycling process of the threshold T, obtained from numerical simulations of the microscopic model defined by Eqs. (1) in a fully connected network of N sites when N increases. When the fraction of inhibitory units $f < 1/2$ we observe the appearance of a hysteresis cycle for large-enough system sizes, that converge to a well-defined one in the limit $N \to \infty$. Hysteresis disappears for $f \geqslant 1/2$ for any value of N.

We found that, after a transient, the number of active inhibitory neurons is proportional to the number of active excitatory units. As a consequence, any solution in a system with both excitatory and inhibitory units and $f < 1/2$ can be mapped to a solution in a purely excitatory case. Then the net effect of the inhibitory units is to rescale the value of T. A moment of reflection allows us to observe that this result is a consequence of having an interaction matrix W whose values depend neither on the nature (i.e., either inhibitory or excitatory) of the presynaptic nor the postsynaptic neurons, and having a fully connected network.

We found a pseudotricritical point at $f_t \simeq 1/2$, which is quite away from biologically relevant fractions (which are about $f = 0.2$). However, as it will be discussed below, the obtained value of f_t is not relevant on it's own, but rather, a consequence of having the same strength for inhibitory and excitatory output connections. A different value of f_t could be obtained if we considered that the inhibitory units had stronger output connections (as frequently assumed in other models [20,21]) without changing qualitatively any of the preceding results.

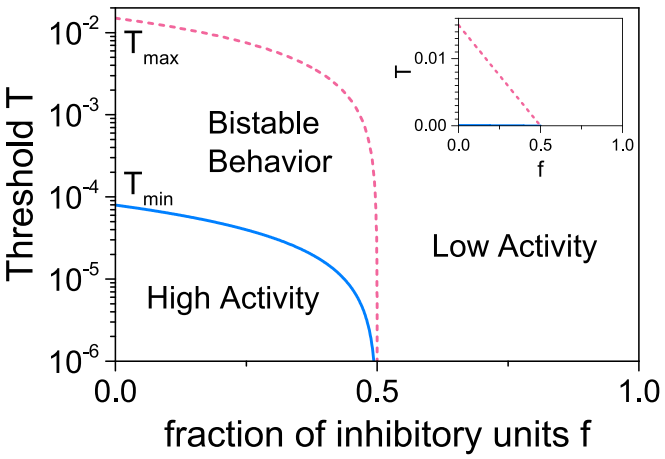

FIG. 8. Dynamical phase diagram (log-linear plot) in the (f, T) space, in the thermodynamic limit ($N \to \infty$ or $\sigma \to 0$). Stability border lines of the bistable region correspond to Eq. (19). The inset shows a linear-linear plot of the same phase diagram.

B. Comparison to other models

The solutions of other neuronal models with excitatory and inhibitory units, either in fully connected or in sparse networks have also been discussed in the literature. There, a variety of mathematical descriptions where considered. For instance, in Ref. [20] integrate-and-fire neurons in a sparsely connected network are considered. In Ref. [21], discrete-time stochastic integrate-and-fire neurons in a fully connected network are considered. In Ref. [17], equations for the rate of activation of a contact process (closely related to neuronal dynamics) are considered. Also, in an early phenomenological description of excitatory and inhibitory neuronal dynamics, differential equations for the activity of neuronal population were considered [22]. It should be stressed that bistable behavior, as observed here, is present in all these models.

In most of such models more sophisticate descriptions of neurons were used; consequently, a larger number of variables and parameters were employed. However, some of them could be related to the present model variables. For instance, instead of having the fraction of inhibitory units as a variable (f), in Refs. [20,21] they fix the proportion to 80% excitatory and 20% inhibitory but let the strength of inhibitory synapses be g times that of the excitatory ones. Then, for each value of g we would get an essentially related value of $f \simeq (g+1)/10$. In particular, the so-called *balanced* system, where the net effect of the excitatory and the inhibitory units has the same magnitude, corresponds to $g_c = 4$ (or $f_t = 1/2$ as discussed here).

For low values of external input, if $g < g_c$ (here, $f < 1/2$), then in Refs. [20,21] they find three solutions in complete agreement with our results. If $g > g_c$, i.e., the *inhibition dominated region*, then they find a single low-activity solution. Other interesting results arise when the intensity if external input [20,21] becomes larger than some critical value, which do not have a clear relation to results presented here. If homeostatic mechanisms are added to the dynamics, then it will converge to a single critical point where scale-free avalanches take place [21].

Regarding the contact process model with inhibitory units, although a richer regime diagram is obtained in Ref. [17], when asymmetric inhibition is considered (inhibitory units do not inhibit inhibitory units), a simple regime is recovered for symmetric inhibition, as in the present case.

If we now consider the dynamics taken by brain's cortical neurons (instead of the simple numerical models described above), then a larger variety of behaviors is obtained, which depends on the cortical region being studied, the species, and many other factors. Nevertheless, inhibition dominated regimes, with *loose* excitatory-inhibitory (E/I) balance are frequent [23]. There the average strength of the excitatory connections, the average strength of the inhibitory connections, their instantaneuos difference, and the threshold are all of the same order of magnitude. As a consequence, the fluctuations in the input signals of a single neuron are of comparable size with their mean values, and spiking is fluctuation dominated (in contrast to *tight* E/I balance) [23]. This scenario is similar to the one already predicted in Ref. [24], where chaotic dynamics is expected as a result of the fluctuating balance. These results differ from those presented here. Notice that a key ingredient in these cases is a sparse network with connectivity (or degree) $\langle k \rangle$ much smaller than network size (i.e., $\langle k \rangle \ll N$), quite different from the fully connected networks considered here.

C. Concluding remarks and future work

From a statistical physics point of view, the presence of a phase transition (i.e., a nonanalytic behavior of the state variables) in a finite system, is not unusual in nonthermodynamical systems [4,25,26], at variance with what happens in thermodynamical ones where nonanalytic behavior can only happen in the thermodynamic limit.

The present example is consistent with predictions of bistable behavior in other models [17,20–22]. Nevertheless, we found that the first-order transition line in the (f, T) space stops at a point (f_t, T_t), being replaced by a continuous crossover between low- and high-activity regions when $f > f_t$, that resembles the finite-size behavior of a continuous phase transition order parameter. In that sense, (f_t, T_t) could be regarded as a pseudotricritical point. However, such pseudocritical behavior for $f > f_t$ completely disappears in the thermodynamic limit $\sigma \to 0$, where the total activity becomes negligible for any value of $T > 0$.

On the other hand, the behavior of the GH model on a fully connected network is expected to reproduce (with the interactions strength properly normalized) the $\langle k \rangle \to N \to \infty$ limit of the GH model on a Watts-Strogatz network, which, for an average degree $\langle k \rangle = 30$ exhibits true tricritical behavior [4]. Therefore, the present results suggest that the critical region of the last model in the large connectivity limit should shrink as the average degree increases and the tricritical fraction of inhibitory units should converge to $1/2$. Moreover, preliminary simulation results indicate that the critical region remains finite (and consequently the triciritical point still exists) in large $N \gg 1$ systems with large connectivity $\langle k \rangle \gg 1$, as long as $\langle k \rangle / N \ll 1$. Works along these lines are in progress and will be published elsewhere. It is worth stressing that tricirical behavior was also observed in a different mean-field model [17].

Finally, we have checked that the proportionality among active excitatory and active inhibitory units holds, at least approximately, when the GH model is simulated on a Watts-Strogatz network (as in Ref. [4]), suggesting that this property does not depend on the network's topology. Furthermore, if this property holds, then it may provide further insights on the so-called *paradoxical effect*, according to which, the external inhibition of inhibitory units may generate responses where both the activity of excitatory and inhibitory units increase and oscillate in phase [27]. An interesting avenue of future research is to study under which conditions this proportionality is maintained in other models and solutions studied in the literature. Also, it would be worth to study under which conditions the solutions including inhibitory units can be mapped to equivalent solutions for purely excitatory neurons.

ACKNOWLEDGMENTS

This work was partially supported by CONICET (Argentina) through Grants PIP No. 1122020010106, by SeCyT (Universidad Nacional de Córdoba, Argentina), and by the NIH (USA) Grant No. 1U19NS107464-01. J.A. is supported by a doctoral fellowship from CONICET (Argentina). This work used Mendieta Cluster from CCAD-UNC, which is part of SNCAD-MinCyT, Argentina.

APPENDIX A: LISTS OF VARIABLES

The list of variable names and their description for the cellular automaton model is included in Table I, while the variables for the dynamical equations are included in Table II.

TABLE I. Neuronal network model variables.

Symbols	Reference
N	Number of neurons
$x_i = 0, 1, 2$	Neuron i state
f	Fraction of inhibitory units
$\epsilon_i = 1\ (-1)$	If neuron i is excitatory (inhib.)
r_1	Spontaneous activation rate ($r_1 = 10^{-3}$)
r_2	Relaxation from refractory rate ($r_2 = 0.3$)
T	Threshold, model's control parameter
W_{ij}	Connection weight (absolute value) among neurons i and j in the original model
w_{ij}	Connection weight (absolute value) used in the fully connected model $w_{ij} = W_{i,j}/N$
β	Weight distribution parameter [Eq. (2)]

TABLE II. Variables used in the dynamical equations.

Symbols	Reference
$\rho_{e/r}$	Density of excited (refractory) excitatory units
$\psi_{e/r}$	Density of excited (refractory) inhibitory units
Σ_e	Activity ($\Sigma_e = \rho_e + \psi_e$)
Σ_r	Total number of refractory units ($\Sigma_r = \rho_r + \psi_r$)
$\Delta_{e/r}$	Auxiliary variables ($\Delta_{e/r} = f\,\rho_{e/r} - (1-f)\psi_{e/r}$)
$\mu_{1,2,3}$	Transition rates
$\eta()$	Sigmoideal function approximation
σ	Mean-square deviation of v_i (see Appendix B)
$\Sigma^*_{e/r}$, $\rho^*_{e/r}$	Stationary values
$\Delta_e^{\max/\min}$	
$\rho_e^{\max/\min}$	Values at the bistability limits
$T^{\max/\min}$	
Σ_e^t, T_t, f_t	Values at the pseudotriciritical point
S	Auxilliary variable. $S = \mu_1\mu_2 + \mu_2\mu_3 + \mu_3\mu_1$
$R(\Sigma_e, f)$	Auxilliary variable; see Eq. (17)
B	Auxilliary variable, $B = \frac{4S(S+\mu_2+\mu_3)}{\mu_2^2\mu_3}$

APPENDIX B: STOCHASTIC TREATMENT

Starting from the neuronal network model, we will *assume* the following transition rates for $x_i(t)$:

$$\begin{aligned} U_i(0 \to 1) &= \mu_1 + \alpha\,\Theta(v_i) \\ U_i(1 \to 2) &= \mu_3 \\ U_i(2 \to 0) &= \mu_2, \end{aligned} \tag{B1}$$

where

$$v_i \equiv \sum_{j=1}^{N} w_{ij}\epsilon_j \delta(x_j(t), 1) - T, \tag{B2}$$

and μ_1, μ_2, μ_3, and α are constants whose value will be derived in the next section. While Eqs. (B1) allow in principle to construct a master equation for the probability $P(\vec{x}, t)$, it would be analytically intractable. Thus, it is convenient to work with macroscopic variables like the number of sites in every state, such as $n_q^E = \sum_{i\in\text{exc}} \delta(x_i, 0)$, $n_e^E = \sum_{i\in\text{exc}} \delta(x_i, 1)$, and $n_r^E = \sum_{i\in\text{exc}} \delta(x_i, 2)$ for excitatory sites (analogously for inhibitory ones).

Using the local transition probabilities Eqs. (B1), we can calculate the transition probabilities for the populations $\vec{\boldsymbol{n}} = (\vec{\boldsymbol{n}}^E, \vec{\boldsymbol{n}}^I) = (n_q^E, n_e^E, n_r^E, n_q^I, n_e^I, n_r^I)$, namely

$$\begin{aligned} U^{E/I}\big(\{n_q^{E/I}, n_e^{E/I}\} \to \{n_q^{E/I} - 1, n_e^{E/I} + 1\}\big) \\ = \sum_{q\ \text{state}} (\mu_1 + \alpha\,\Theta) \approx n_q^{E/I}(\mu_1 + \alpha\,\langle\Theta\rangle) \\ U^{E/I}\big(\{n_e^{E/I}, n_r^{E/I}\} \to \{n_e^{E/I} - 1, n_r^{E/I} + 1\}\big) \\ = \sum_{e\ \text{state}} \mu_3 = n_e^{E/I}\mu_3 \\ U^{E/I}\big(\{n_r^{E/I}, n_q^{E/I}\} \to \{n_r^{E/I} - 1, n_q^{E/I} + 1\}\big) \\ = \sum_{r\ \text{state}} \mu_2 = n_r^{E/I}\mu_2. \end{aligned} \tag{B3}$$

The approximation made in the first equation $\Theta \to \langle\Theta(v_i)\rangle$ where the average is over stochastic variable v_i, is expected to be valid for a mean-field system. These rates give rise to the Master equation

$$\begin{aligned} \frac{\partial}{\partial t}P(\vec{\boldsymbol{n}}, t) = {} & \mu_3\big(n_e^E + 1\big)P\big(n_q^E, n_e^E + 1, n_r^E - 1, \vec{\boldsymbol{n}}^I, t\big) \\ & + \mu_2\big(n_r^E + 1\big)P\big(n_q^E - 1, n_e^E, n_r^E + 1, \vec{\boldsymbol{n}}^I, t\big) \\ & + (\mu_1 + \alpha\,\langle\Theta\rangle)\big(n_q^E + 1\big) \\ & \times P\big(n_q^E + 1, n_e^E - 1, n_r^E, \vec{\boldsymbol{n}}^I, t\big) \\ & - \big[\mu_3 n_e^E + \mu_2 n_r^E + (\mu_1 + \alpha\,\langle\Theta\rangle)n_q^E\big]P(\vec{\boldsymbol{n}}, t) \\ & + (\text{analogous terms for inhibitory}). \end{aligned} \tag{B4}$$

Using a Kramers-Moyal expansion [16] a Fokker-Planck equation for the densities $\vec{\boldsymbol{y}} = \vec{\boldsymbol{n}}/N$ can be derived in the limit $N \to \infty$, namely

$$\frac{\partial}{\partial t}P(\vec{\boldsymbol{y}}, t) = -\sum_i \frac{\partial}{\partial y_i}[a_i P(\vec{\boldsymbol{y}}, t)] + \frac{1}{2}\sum_{ij}\frac{\partial^2}{\partial y_i \partial y_j}[b_{ij}P(\vec{\boldsymbol{y}}, t)], \tag{B5}$$

where subindexes run over six components (three excitatory and three inhibitory) and [16]

$$\begin{aligned} \vec{\boldsymbol{a}} &= (\vec{\boldsymbol{a}}^E, \vec{\boldsymbol{a}}^I) = \big(a_q^E, a_e^E, a_r^E, a_q^I, a_e^I, a_r^I\big) \\ &= (\mathcal{R}^E - \mathcal{Q}^E, \mathcal{Q}^E - \mathcal{E}^E, \mathcal{E}^E - \mathcal{R}^E, \mathcal{R}^I - \mathcal{Q}^I, \mathcal{Q}^I - \mathcal{E}^I, \mathcal{E}^I - \mathcal{R}^I) \end{aligned} \qquad \hat{b} = \begin{pmatrix} \hat{b}^E & 0 \\ 0 & \hat{b}^I \end{pmatrix} \tag{B6}$$

with

$$\hat{b}^{E/I} = \frac{1}{N}\begin{pmatrix} \mathcal{E}^{E/I} + \mathcal{Q}^{E/I} & -\mathcal{Q}^{E/I} & -\mathcal{E}^{E/I} \\ -\mathcal{Q}^{E/I} & \mathcal{Q}^{E/I} + \mathcal{R}^{E/I} & -\mathcal{R}^{E/I} \\ -\mathcal{E}^{E/I} & -\mathcal{R}^{E/I} & \mathcal{E}^{E/I} + \mathcal{R}^{E/I} \end{pmatrix} \begin{matrix} e \\ q \\ r \end{matrix} \qquad \begin{aligned} \mathcal{Q}^{E/I} &= y_q^{E/I}(\mu_1 + \alpha\,\langle\Theta\rangle) \\ \mathcal{E}^{E/I} &= y_e^{E/I}\mu_3 \\ \mathcal{R}^{E/I} &= y_r^{E/I}\mu_2. \end{aligned} \tag{B7}$$

Under the Itô interpretation [16], we can derive from Eq. (B5) the stochastic differential equation

$$d\vec{\boldsymbol{y}} = \vec{\boldsymbol{A}}(\vec{\boldsymbol{y}}, t)dt + \hat{B}(\vec{\boldsymbol{y}}, t)d\vec{\boldsymbol{\xi}}(t), \tag{B8}$$

where $\vec{A} = (\vec{a}^E, \vec{a}^I)$, $(\hat{B}\hat{B}^\intercal)_{ij} = b_{ij}$, and $\vec{\xi}$ is a multivariable Wiener process. Averaging over the noise and defining $\dot{\vec{\rho}} \equiv \langle \dot{\vec{y}}^E \rangle$ and $\dot{\vec{\psi}} \equiv \langle \dot{\vec{y}}^I \rangle$, we obtained

$$\begin{aligned}
\dot{\rho}_q &= \mu_2 \rho_r - (\mu_1 + \alpha \langle \Theta \rangle)\rho_q \\
\dot{\rho}_e &= (\mu_1 + \alpha \langle \Theta \rangle)\rho_q - \mu_3 \rho_e \\
\dot{\rho}_r &= \mu_3 \rho_e - \mu_2 \rho_r \\
\dot{\psi}_q &= \mu_2 \psi_r - (\mu_1 + \alpha \langle \Theta \rangle)\psi_q \\
\dot{\psi}_e &= (\mu_1 + \alpha \langle \Theta \rangle)\psi_q - \mu_3 \psi_e \\
\dot{\psi}_r &= \mu_3 \psi_e - \mu_2 \psi_r,
\end{aligned} \tag{B9}$$

where $\rho_k = \langle n_k^E / N \rangle$ and $\psi_k = \langle n_k^I / N \rangle$ $(k = q, e, r)$, as in main text. Finally, using the relationships

$$\begin{aligned}
N &= N_e + N_i \\
\rho_e + \rho_q + \rho_r &= \frac{N_e}{N} = 1 - f \\
\psi_e + \psi_q + \psi_r &= \frac{N_i}{N} = f,
\end{aligned} \tag{B10}$$

we get

$$\begin{aligned}
\dot{\rho}_e &= (1 - f - \rho_e - \rho_r)(\mu_1 + \alpha \langle \Theta \rangle) - \mu_3 \rho_e \\
\dot{\rho}_r &= \mu_3 \rho_e - \mu_2 \rho_r \\
\dot{\psi}_e &= (f - \psi_e - \psi_r)(\mu_1 + \alpha \langle \Theta \rangle) - \mu_3 \psi_e \\
\dot{\psi}_r &= \mu_3 \psi_e - \mu_2 \psi_r.
\end{aligned} \tag{B11}$$

Assuming that v_i behaves as a Gaussian variable we can calculate the average

$$\begin{aligned}
\langle \Theta \rangle &= \frac{1}{\sigma\sqrt{2\pi}} \int_{-\infty}^{\infty} \Theta(v_i) e^{-\frac{(v_i - \mu)^2}{2\sigma^2}} \mathrm{d}v_i \\
&= \frac{1}{2}\left[1 + \mathrm{erf}\left(\frac{\mu}{\sqrt{2}\sigma}\right)\right] \equiv \eta(\mu/\sigma),
\end{aligned} \tag{B12}$$

where $\sigma^2 = \mathrm{Var}(v_i)$ and

$$\begin{aligned}
\mu = \langle v_i \rangle &= \left\langle \sum_{j=1}^{N} w_{ij} \epsilon_j \delta(x_j(t), 1) - T \right\rangle \\
&\approx \frac{\omega}{N} \left\langle \sum_{j \in \mathrm{exc}}^{N_{\mathrm{exc}}} \delta(x_j(t), 1) - \sum_{j \in \mathrm{inhib}}^{N_{\mathrm{inhib}}} \delta(x_j(t), 1) \right\rangle - T \\
&\approx \omega(\rho_e - \psi_e) - T,
\end{aligned}$$

where

$$\omega \equiv \langle W_{ij} \rangle. \tag{B13}$$

From Eq. (2), we get $\omega = 1/\beta$. We have also assumed that

$$\langle w_{ij} \epsilon_j \delta(x_j(t), 1) \rangle \approx \langle w_{ij} \rangle \langle \epsilon_j \delta(x_j(t), 1) \rangle.$$

We checked the validity of this approximation by performing numerical simulations of the microscopic GH model in a fully connected network for different values of T and N. We found that the correlations between the quenched disorder variables and $\delta(x_j(t), 1)$ were indeed negligible for large-enough values of N. Since the results are not expected to depend on the specific form of the sigmoidal function $\eta(x)$ as long as it has the same asymptotic behaviors for $x \to \pm\infty$, in what follows we replaced η in Eq. (B12) by the simplified form

$$\eta(x) = \frac{e^{2x}}{1 + e^{2x}}. \tag{B14}$$

Replacing the above results into Eqs. (B11) we obtained

$$\dot{\rho}_e = (1 - f - \rho_e - \rho_r) \times \left\{ \mu_1 + \alpha\, \eta\left[\frac{\omega(\rho_e - \psi_e) - T}{\sigma} \right] \right\} - \mu_3 \rho_e, \tag{B15a}$$

$$\dot{\rho}_r = \mu_3 \rho_e - \mu_2 \rho_r, \tag{B15b}$$

$$\dot{\psi}_e = (f - \psi_e - \psi_r) \times \left\{ \mu_1 + \alpha\, \eta\left[\frac{\omega(\rho_e - \psi_e) - T}{\sigma} \right] \right\} - \mu_3 \psi_e, \tag{B15c}$$

$$\dot{\psi}_r = \mu_3 \psi_e - \mu_2 \psi_r, \tag{B15d}$$

which are similar to Eqs. (4) but still depend on α.

APPENDIX C: MODEL PARAMETRIZATION

The continuous time stochastic process defined by Eqs. (B1) can be described as a set of coupled, constant rate jump (or Poisson) processes, each one corresponding to the transition of a single neuron. The Poisson processes are coupled in the sense that an event generated by one process may alter the other process by changing their rates [28]. The transition probabilities of a single neuron i in this continuous time process are then given by [28]

$$\begin{aligned}
\Pi_i(0 \to 1) &= U_i(0 \to 1)/v_i \\
\Pi_i(1 \to 2) &= U_i(1 \to 2)/v_i \\
\Pi_i(2 \to 0) &= U_i(2 \to 0)/v_i,
\end{aligned}$$

where

$$v_i = U_i(0 \to 1) + U_i(1 \to 2) + U_i(2 \to 0).$$

Now the basic assumption is that, at least as far as the stationary properties are concerned, the parallel dynamics where the state of all the neurons at time $t + 1$ are updated simultaneously from their state at time t (according to the transition probabilities given by Eqs. (B1) is equivalent to a sequential update, in a way analogous to the single spin flip rules used in Monte Carlo simulations of discrete spin systems [29]. In other words, neurons in such rules would be updated one by one, where each update may affect the probabilities of the next one. In such a sense, the macroscopic timescale to be compared with the parallel dynamics time unit would be a set of N single update trials (the "Monte Carlo step"). We checked numerically the stationary properties of both dynamics in different regions of the parameters space for the fully connected model. We verified that both dynamics give qualitatively always the same results, where the quantitative differences become negligible close enough to the dynamical transition regions (not shown). Under the assumption of such equivalency, we can assume that

$$\Pi_i(0 \to 1) = P_i(0 \to 1), \tag{C1}$$

$$\Pi_i(1 \to 2) = P_i(1 \to 2), \tag{C2}$$

$$\Pi_i(2 \to 0) = P_i(2 \to 0), \tag{C3}$$

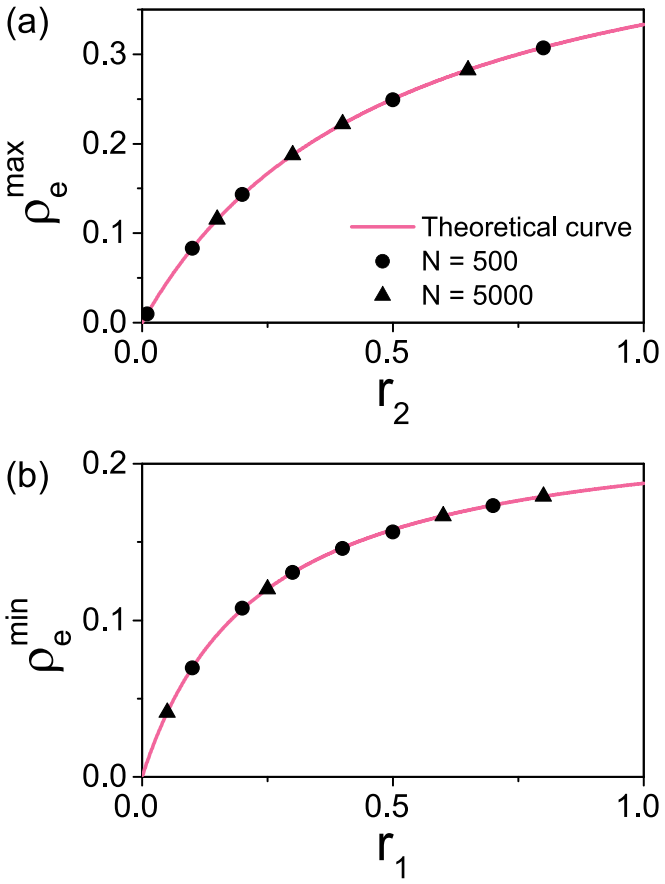

FIG. 9. (a) Maximum activity as a function of r_2 for $r_1 = 10^{-3}$. (b) Minimum activity as a function of r_1 for $r_2 = 0.3$. Numerical values of fully connected simulations are plotted for two network sizes in both cases. Theoretical results were obtained for $\sigma^2 = 10^{-7}$.

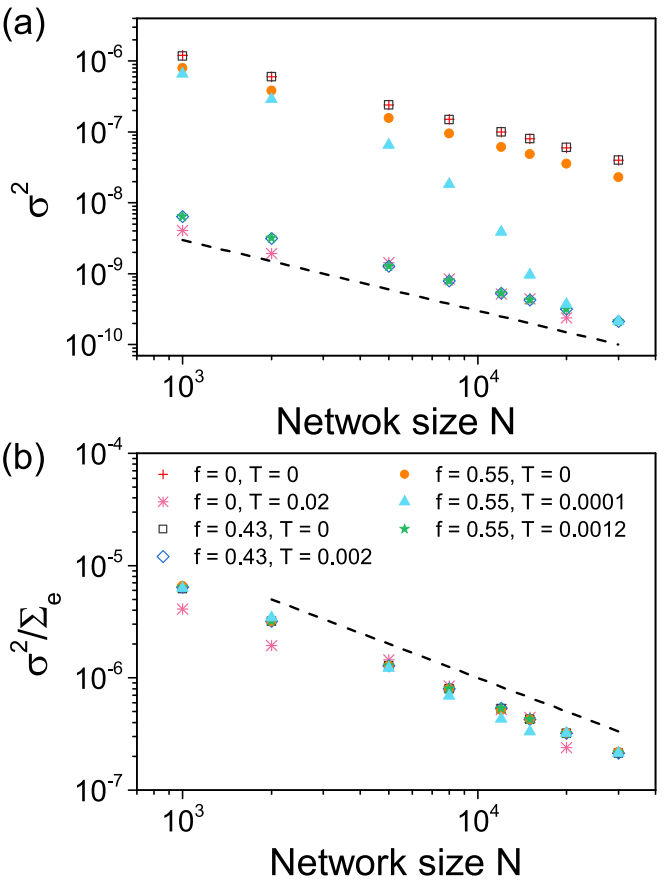

FIG. 10. Finite-size scaling of the variance σ^2 for different combinations of the parameters (f, T). (a) σ^2 as a function of the networks size N. (b) σ^2/Σ_e as a function of N. The dashed lines are power laws proportional to N^{-1}.

where the transition probabilities P_i are given by Eqs. (1). Hence

$$\frac{\mu_1 + \alpha\,\Theta}{\nu_i} = 1 - (1 - r_1)(1 - \Theta), \tag{C4}$$

$$\frac{\mu_3}{\nu_i} = 1, \tag{C5}$$

$$\frac{\mu_2}{\nu_i} = r_2. \tag{C6}$$

From Eq. (C4) we have that $\mu_1/\nu_i = r_1$ when $\Theta = 0$ and $(\mu_1 + \alpha)/\nu_i = 1$ when $\Theta = 1$. Therefore

$$\mu_1 = \frac{\alpha\, r_1}{1 - r_1}. \tag{C7}$$

Combining Eqs. (C5) and (C6) with the last one we obtain

$$\mu_2 = \frac{\alpha\, r_2}{1 - r_1}, \tag{C8}$$

$$\mu_3 = \frac{\alpha}{1 - r_1}. \tag{C9}$$

Since $\mu_{1,2,3}$ are proportional to α, then the time evolution of each variable in Eq. (B15) is proportional to α. Without loss of generality we may rescale time in such way that $\alpha = 1$, so we finally arrive to Eqs. (4) of main text. Expressions (C7)–(C9) can be checked by considering some limiting cases of the dynamical equations (7) for $f = 0$. As explained in Sec. III A, the stationary solutions of Eqs. (7) present a discontinuous transition from a high-activity phase to a low-activity one as the threshold T is increased, with the presence of hysteresis (see also Appendix E). The associated maximum ($T \to 0$) and minimum ($T \to \infty$) values of the density of active sites ρ_e correspond to the stationary solutions Eqs. (7) when $\eta \to 0$ and $\eta \to 1$, respectively. Combining such solutions with Eqs. (C7)–(C9) (assuming $\alpha = 1$) we obtain the expressions

$$\rho_e^{\min} = \frac{r_2}{2r_2 + 1} \qquad \rho_e^{\max} = \frac{1}{1 + 1/r_1 + 1/r_2}, \tag{C10}$$

which are independent of σ and therefore from the system size. These can be compared with numerical simulation results from the microscopic model. The comparison shown in Fig. 9 exhibits a full agreement in the whole range of values of r_1 and r_2.

APPENDIX D: FINITE-SIZE SCALING

We analyzed the finite-size scaling of the variance $\sigma^2 = \langle v_i^2 \rangle - \langle v_i \rangle^2$ for the microscopic model defined on a fully

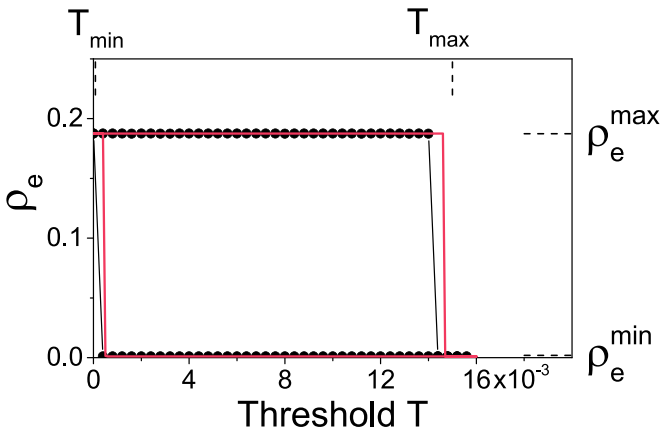

FIG. 11. Comparison between a hysteresis loop generated with Greenberg-Hastings dynamics over a fully connected network of size $N = 30\,000$ (black line-dots) and one obtained from the mean-field model with parameter $\sigma = 10^{-4}$ (solid pink line).

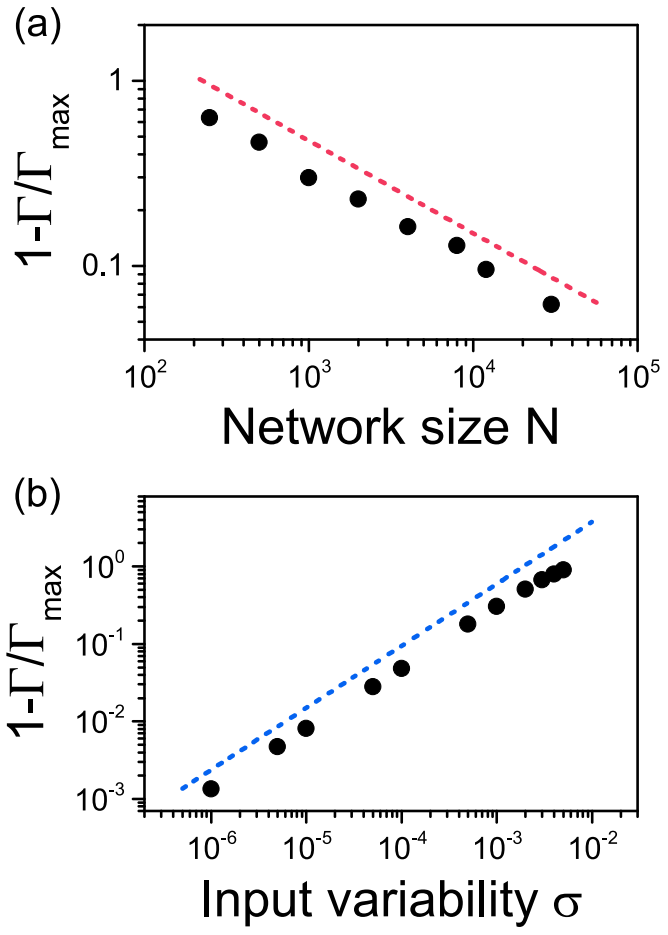

FIG. 12. Hysteresis width Γ tends to its maximum value $\Gamma_{\max}$ in the thermodynamic limit ($N \to \infty$ or $\sigma \to 0$) as power law both for the numerical simulation and for the mean-field equations. (a) Numerical simulation results. The pink dashed line is a power law in the network size $\sim N^{-0.5}$. (b) Mean-field equations results. The blue dashed line is a power law in the σ parameter $\sim \sigma^{0.8}$.

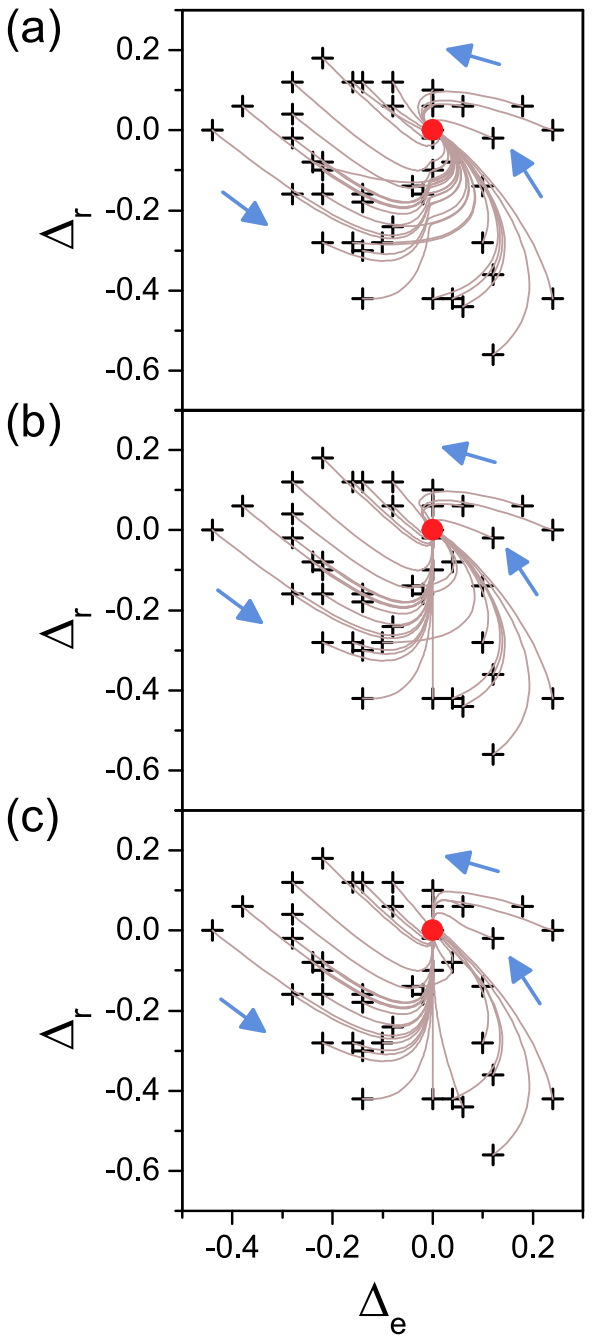

FIG. 13. Evolution of the auxilliary variables Δ_e and Δ_r computed the from full system of equations, Eqs. (11) for different parameters and initial conditions. The trajectories for Δ_r as a function of Δ_e are shown for $f = 0.3$, and 3 values of T: $T = 0$ (a), $T = 0.004$ (b), and $T = 0.02$ (c). We computed trajectories for all the possible combinations of the following initial values: $\rho_e = 0, 0.2, \ldots, 1$; $\rho_r = 0, 0.2, \ldots, 1 - \rho_e$; $\psi_e = 0, 0.2, \ldots, 1$; and $\psi_r = 0, 0.2, \ldots, 1 - \psi_e$, making a total of 225 trajectories for each value of T. For clarity, we only show approximately 20% of the trajectories, randomly selected. Black crosses correspond to different initial conditions and the red circles correspond to the final conditions. The arrows show the instantaneous evolution of a few selected trajectories. Notice that different combinations of $\rho_{e/r}$ and $\psi_{e/r}$ may lead to the same values of $\Delta_{e/r}$.

connected network with N sites, where the variables v_i are given by Eq. (B2).

It is assumed that σ is independent of the site i. The results are shown in Fig. 10, for different values of the parameters (f, T). We see, that in all cases $\sigma^2 \propto C/N$, where $C \propto \Sigma_e$ (see Fig. 10).

APPENDIX E: MULTISTABILITY

To verify the existence of hysteresis we solved numerically the dynamical equations (7) for $f = 0$ for different values of σ. We verified that for small-enough values of σ the properties of the stationary state of Eqs. (7) are almost insensitive to σ for a wide range (around two orders of magnitude) of values of it. We performed a loop of increasing-decreasing T solving Eqs. (7) using the RK method. For each value of T, we run the RK algorithm until the system reaches a stationary state and record the stationary value of ρ_e before changing $T \to T \pm \Delta T$ ($\Delta T \sim 1.5 \times 10^{-5}$) and restart the RK algorithm with the previous state as the new initial condition. We also performed a similar loop in a numerically simulated GH model in a fully connected network. In this case, for every value of T, we discard the first $t = 500$ steps and average the fraction of active sites over 10^3–10^4 steps before changing T, taking the last configuration as the initial one for the new value of T. In Fig. 11 we compare two loops of ρ_e vs T for both systems, one with $N = 30\,000$ and the other with $\sigma = 10^{-4}$. We also show in Fig. 12 the hysteresis width Γ[2] as a function of the network size N for numerical simulated GH model loops or as a function of σ for numerical solutions of the Eqs. (7). We find that Γ converges through a power law to its limit value $\Gamma_{\max} = T_{\max} - T_{\min}$ for $N \to \infty$ and $\sigma \to 0$ in each case, where $T_{\min}$ and $T_{\max}$ are given by Eqs. (19) of main text.

We now analyze the unstable solution for the case $f = 0$. The unstable solution in the general case can be derived in a similar way.

In the limit $\sigma \to 0$, $\eta(\frac{\omega\rho_e - T}{\sigma})$ can only have three values: 0, 1, and 1/2. The first two correspond to stable solutions. We found that the third one is close to the unstable solution presented by the model. To find that solution, we approximated $\eta(x)$ by the first two terms of its Taylor series expansion, $\frac{1}{2}(1 + x)$, obtaining the equation for the stationary solution

$$\left[1 - \rho_e\left(1 + \frac{\mu_3}{\mu_2}\right)\right]\left(\mu_1 + \frac{1}{2} + \frac{\omega\rho_e - T}{2\sigma}\right) - \rho_e\mu_3 = 0. \tag{E1}$$

This is second degree polynomial on ρ_e. It has two solutions, one for which $\rho_e > \rho_e^{\max}$, and the other, which is close to $\frac{T}{\omega}$. This solution is already plotted in Fig. 2.

APPENDIX F: STABILITY OF $\Delta_{e/r} = 0$

The equations for $\Delta_{e/r}$ are

$$\dot{\Delta}_e = (-\mu_3 - \mathcal{N})\Delta_e - \mathcal{N}\Delta_r, \tag{F1}$$

$$\dot{\Delta}_r = \mu_3\Delta_e - \mu_2\Delta_r. \tag{F2}$$

In the stationary state, the equations for $\Delta_{e/r}$ read

$$\begin{aligned}(-\mu_3 - \mathcal{N})\Delta_e^* - \mathcal{N}\Delta_r^* &= 0\\ \mu_3\Delta_e^* - \mu_2\Delta_r^* &= 0.\end{aligned} \tag{F3}$$

Since we are in the stationary state $\mathcal{N}$ is constant. Hence, we can consider the above system as two linear equations on $\Delta_{e/r}$. Both equations are linearly independent since the first one has two negative coefficients and the second one has one positive and the other negative. Then, they have only one solution, which is $\Delta_{e/r}^* = 0$ (for any value of $\mathcal{N}$). We now consider their stability. We can write

$$\Delta_{e/r} = \Delta_{e/r}^* + \delta\Delta_{e/r}, \tag{F4}$$

$$\Sigma_{e/r} = \Sigma_{e/r}^* + \delta\Sigma_{e/r}, \tag{F5}$$

where $\delta\Sigma_{e/r}$ and $\delta\Delta_{e/r}$ are the (small) fluctuations of $\Delta_{e/r}$ and $\Sigma_{e/r}$ around their stationary values. We can also write $\mathcal{N} = \mathcal{N}^* + \delta\mathcal{N}$, with $\delta\mathcal{N} = \frac{\partial\mathcal{N}}{\partial\Sigma_e}\delta\Sigma_e + \frac{\partial\mathcal{N}}{\partial\Delta_e}\delta\Delta_e$. We then get

$$\begin{aligned}\delta\dot{\Delta}_e &= (-\mu_3 - \mathcal{N}^*)\delta\Delta_e - \delta\mathcal{N}\underbrace{\Delta_e^*}_{0} - \mathcal{N}^*\\ &+ \delta\Delta_r - \delta\mathcal{N}\underbrace{\Delta_r^*}_{0} + O(\delta^2)\\ \delta\dot{\Delta}_r &= \mu_3\delta\Delta_e - \mu_2\delta\Delta_r + O(\delta^2).\end{aligned} \tag{F6}$$

This can be written in matrix form

$$\begin{pmatrix}\delta\dot{\Delta}_e\\ \delta\dot{\Delta}_R\end{pmatrix} = \begin{pmatrix}-\mu_3 - \mathcal{N}^* & -\mathcal{N}^*\\ \mu_3 & -\mu_2\end{pmatrix} \cdot \begin{pmatrix}\delta\Delta_e\\ \delta\Delta_R\end{pmatrix}.$$

The eigenvalues of the matrix are $\lambda_\pm = \frac{-\mathcal{N}* - \mu_3 - \mu_2}{2} \pm \frac{1}{2}\sqrt{(\mathcal{N}^* - \mu_3 - \mu_2)^2 - 4\mu_2\mu_3}$, which have negative real part, so the solution is stable. We have computed numerically the evolution of the $\rho_{e/r}$ and $\psi_{e/r}$, Eqs. (7), for different values of f and T, and several different initial conditions. The results show that the different trajectories converge to $\Delta_{e/r} = 0$. In Fig. 13 we show some examples of these trajectories for $f = 0.3$, and three values of T: $T = 0$ (where the only stationary solution corresponds to $\Sigma_e \simeq \Sigma_e^{\max}$), $T = 0.004$ (where $\Sigma_e \simeq \Sigma_e^{\max}$ and $\Sigma_e \simeq \Sigma_e^{\min}$ coexist), and $T = 0.02$ (where $\Sigma_e \simeq \Sigma_e^{\min}$).

[2]The hysteresis width Γ is calculated as the difference between the threshold values in the loop edges. Those thresholds are an average between the values in the upper and lower corners of the loop edges.

[1] M. Henkel, H. Hinrichsen, and S. Lübeck, *Non-Equilibrium Phase Transitions* (Springer, Berlin, 2008), Vol. 1.

[2] J. Marro and R. Dickman, *Nonequilibrium Phase Transitions in Lattice Models* (Cambridge University Press, Cambridge, UK, 1999).

[3] G. Ódor, Universality classes in nonequilibrium systems, Rev. Mod. Phys. **76**, 663 (2004).

[4] J. Almeira, T. S. Grigera, D. R. Chialvo, and S. A. Cannas, Tricritical behavior in a neural model with excitatory and inhibitory units, Phys. Rev. E **106**, 054140 (2022).

[5] A. Haimovici, E. Tagliazucchi, P. Balenzuela, and D. R. Chialvo, Brain organization into resting state networks emerges at criticality on a model of the human connectome, Phys. Rev. Lett. **110**, 178101 (2013).

[6] M. Zarepour, J. I. Perotti, O. V. Billoni, D. R. Chialvo, and S. A. Cannas, Universal and nonuniversal neural dynamics on small world connectomes: A finite-size scaling analysis, Phys. Rev. E **100**, 052138 (2019).

[7] M. M. S. Diaz, E. J. A. Trejo, D. A. Martin, S. A. Cannas, T. S. Grigera, and D. R. Chialvo, Similar local neuronal dynamics may lead to different collective behavior, Phys. Rev. E **104**, 064309 (2021).

[8] J. M. Greenberg and S. P. Hastings, Spatial patterns for discrete models of diffusion in excitable media, SIAM J. Appl. Math. **34**, 515 (1978).

[9] J. M. Beggs and D. Plenz, Neuronal avalanches in neocortical circuits, J. Neurosci. **23**, 11167 (2003).

[10] D. R. Chialvo, Emergent complex neural dynamics, Nat. Phys. **6**, 744 (2010).

[11] T. Mora and W. Bialek, Are biological systems poised at criticality? J. Stat. Phys. **144**, 268 (2011).

[12] J. Wilting and V. Priesemann, 25 years of criticality in neuroscience—Established results, open controversies, novel concepts, Curr. Opin. Neurobiol. **58**, 105 (2019).

[13] M. Girardi-Schappo, Brain criticality beyond avalanches: open problems and how to approach them, J. Phys. Complex. **2**, 031003 (2021).

[14] J. O'Byrne and K. Jerb, How critical is brain criticality? Trends Neurosci. **45**, 820 (2022).

[15] P. Hagmann, L. Cammoun, X. Gigandet, R. Meuli, C. J. Honey, V. J. Wedeen, and O. Sporns, Mapping the structural core of human cerebral cortex, PLoS Biol. **6**, e159 (2008).

[16] C. Gardiner, *Stochastic Methods, A Handbook for the Natural and Social Sciences*, Springer Series in Synergetics (Springer, Berlin, 2009).

[17] R. Corral López, V. Buendía, and M. A. Muñoz, Excitatory-inhibitory branching process: A parsimonious view of cortical asynchronous states, excitability, and criticality, Phys. Rev. Res. **4**, L042027 (2022).

[18] G. Barzon, G. Nicoletti, B. Mariani, M. Formentin and S. Suweis, Criticality and network structure drive emergent oscillations in a stochastic whole-brain model, J. Phys. Complex. **3**, 025010 (2022).

[19] R. P. Rocha, L. Koçillari, S. Suweis *et al.*, Homeostatic plasticity and emergence of functional networks in a whole-brain model at criticality, Sci. Rep. **8**, 15682 (2018).

[20] N. Brunel, Dynamics of sparsely connected networks of excitatory and inhibitory spiking neurons, J. Comput. Neurosci. **8**, 183 (2000).

[21] M. Girardi-Schappo, L. Brochini, A. A. Costa, T. T. A. Carvalho and O. Kinouchi, Synaptic balance due to homeostatically self-organized quasicritical dynamics, Phys. Rev. Res. **2**, 012042(R) (2020).

[22] H. R. Wilson and J. D. Cowan, Excitatory and inhibitory interactions in localized populations of model neurons, Biophys. J. **12**, 1 (1972).

[23] Y. Ahmadian and K. D. Miller, What is the dynamical regime of cerebral cortex? Neuron **109**, 3373 (2021).

[24] C. van Vreeswijk and H. Sompolinsky, Chaos in neuronal networks with balanced excitatory and inhibitory activity, Science **274**, 1724 (1996).

[25] P. Serra and J. M. Stilck, Polymer model with annealed dilution on the square lattice: A transfer matrix study, Phys. Rev. E **49**, 1336 (1994).

[26] A. Leviatan, First-order quantum phase transition in a finite system, Phys. Rev. C **74**, 051301(R) (2006).

[27] M. V. Tsodyks, W. E. Skaggs, T. J. Sejnowski and B. L. McNaughton, Paradoxical effects of external modulation of inhibitory interneurons, J. Neurosci. **17**, 4382 (1997).

[28] N. Masuda and C. Vestergaard, *Gillespie Algorithms for Stochastic Multiagent Dynamics in Populations and Networks*, Elements in the Structure and Dynamics of Complex Networks (Cambridge University Press, Cambridge, UK, 2023).

[29] D. P. Landau and K. Binder, *Monte-Carlo Simulations in Statistical Physics* (Cambridge University Press, Cambridge, UK, 2009).